Tellus (1978), 30, 229–239

A finite element model of a moist atmospheric boundary layer: Part II—Method of solution

By M. J. MANTON, *CSIRO, Division of Cloud Physics, P.O. Box 134, Epping, N.S.W. 2121, Australia*

(Manuscript received November 15, 1976; in final form May 2, 1977)

ABSTRACT

A finite element model is presented in order to solve a set of equations which describe the behaviour of moist, deep convection. The method employs elements spanning both time and space, and a variable time step and mesh size can be used. The equation for the pressure is solved in precisely the same manner as that used for the other dependent variables. An artificial, one-dimensional boundary layer flow, in which a mixed layer capped by an inversion is stabilized by cooling at the ground, is solved. The solution is found not to depend significantly upon the time step or the mesh size.

1. Introduction

In Part I of this work (Manton, 1978a), a consistent system of equations is derived to predict the behaviour of the first moments of the dependent variables for moist, deep convection. The covariances of the dependent variables in the system are modelled by means of an eddy diffusivity which is proportional to the turbulent kinetic energy and a characteristic time scale of the turbulence (Kolmogorov, 1942). In this manner the behaviour of the covariances is predicted for all stability conditions without the introduction of many additional differential equations. The system of equations also accounts for fluctuations in the liquid water content by approximating the total water (vapour plus liquid) content by a random binary-switching process.

Equations of this type are solved traditionally by finite difference methods. However, finite difference methods employ different techniques for parabolic and elliptic equations: the dependent variables of parabolic equations usually are given explicitly while those of elliptic equations are not. Thus the pressure, which is governed by an elliptic equation, must be calculated by a technique different from that used to obtain the other dependent variables, which are governed by parabolic equations. A further inconvenience associated with finite difference methods is that their accuracy is maintained only when they are applied with a uniform mesh. This problem can be accommodated by explicitly transforming the dependent variables such that a uniform mesh is used with the transformed variables (Yamada and Mellor, 1975). (We note that nested meshes of different sizes have been used with upstream finite differences (Walsh, 1974).)

On the other hånd, a finite element method, employing linear interpolation in both space and time (Manton, 1978b), can be applied to both parabolic and elliptic equations. Thus all the dependent variables are obtained consistently by the same technique. Being a finite element method, it can be used with a non-uniform mesh and yet retain its overall accuracy. The method of solution is stable for all time increments; when applied to the one-dimensional diffusion equation it is found to be comparable with the implicit Crank-Nicolson finite difference scheme (Manton, 1978b). The purpose of the present work is to show that the finite element method can be applied successfully to solve atmospheric boundary layer flows.

The finite element method is used to solve the model equations of Part I for a one-dimensional boundary layer; that is, the dependent variables are assumed to be statistically homogeneous over a horizontal plane so that the ensemble average values vary only in the vertical direction. Then the ensemble average corresponds to an average over a horizontal plane. Such models yield predictions which compare favourably with some observations in the absence of condensation (Wyngaard and Coté, 1974; Yamada and Mellor, 1975). Because the present work is concerned with the internal consistency of the model rather than with detailed comparison with observations, we introduce a further simplification: Coriolis forces and subsidence are neglected so that there is only one mean velocity component. The problem solved is artificial, but it provides a simple means of testing the ability of the solution method to handle condensation, diffusion and shear.

It is found that the solution method produces results which are relatively insensitive to the spatial mesh size and time step. Although the method of solution is adequate, there may be some doubt about the ability of the model equations, involving an eddy diffusivity, to represent well-mixed layers which are formed by turbulence in a stably stratified fluid. We show finally that the present model is able to predict the deepening of a well-mixed layer by entrainment across an inversion.

2. Equations of motion

We consider an atmospheric boundary layer which is statistically homogeneous over a horizontal plane so that the average properties of the dependent variables vary only in the vertical direction and in time; that is, they are functions of x_3 and t. Moreover the only non-zero mean velocity component is the horizontal velocity $\overline{u}_1$ which acts in the x_1-direction. Thus the model differential equations derived in Part I (Manton, 1978a) reduce to

$$\frac{\partial \overline{u}_1}{\partial t} - \frac{\partial}{\partial x_3}\left(K\frac{\partial \overline{u}_1}{\partial x_3}\right) + \frac{1}{\bar{p}}\frac{\partial \bar{p}}{\partial x_1} = 0, \tag{2.1}$$

$$\frac{\partial \overline{\theta}_L}{\partial t} - a_3\frac{\partial}{\partial x_3}\left(K\frac{\partial \overline{\theta}_L}{\partial x_3}\right) = 0, \tag{2.2}$$

$$\frac{\partial \overline{q}_t}{\partial t} - a_3\frac{\partial}{\partial x_3}\left(K\frac{\partial \overline{q}_t}{\partial x_3}\right) = 0, \tag{2.3}$$

$$\frac{\partial E}{\partial t} - \frac{\partial}{\partial x_3}\left(K\frac{\partial E}{\partial x_3}\right) + \frac{a_1 E}{\tau} + K\left\{a_3 N_3 - \left(\frac{\partial \overline{u}_1}{\partial x_3}\right)^2\right\} = 0, \tag{2.4}$$

$$\frac{\partial \overline{q_t'^2}}{\partial t} - a_3\frac{\partial}{\partial x_3}\left(K\frac{\partial \overline{q_t'^2}}{\partial x_3}\right) + \frac{a_6 \overline{q_t'^2}}{\tau} - 2a_3 K\left(\frac{\partial \overline{q}_t}{\partial x_3}\right)^2 = 0, \tag{2.5}$$

$$\frac{\partial \bar{p}}{\partial x_3} + \bar{p}\left(g + \frac{2}{3}\frac{\partial E}{\partial x_3}\right)\Big/ R_a \overline{T}_v = 0, \tag{2.6}$$

where $\overline{\theta}_L$ is an average potential temperature; $\overline{q}_t$ and $\overline{q_t'^2}$ are the mean and variance of the total water (liquid plus vapor) specific humidity; E is the average turbulent kinetic energy per unit mass; $\bar{p}$ is the average pressure. In these equations, the eddy diffusivity K is given by

$$K = a_2|E|\tau, \tag{2.7}$$

where the turbulent time scale τ satisfies the equation

$$\tau^{-2} = \begin{cases} a_4 N_3, & N_3 \geqslant (\partial\overline{u}_1/\partial x_3)^2 \times Ri_{\text{crit}}, \\ (\partial\overline{u}_1/\partial x_3)^2 - a_3 N_3, & 0 < N_3 < (\partial\overline{u}_1/\partial x_3)^2 \times Ri_{\text{crit}}, \\ (\partial\overline{u}_1/\partial x_3)^2 - a_5 N_3, & N_3 \leqslant 0, \end{cases} \tag{2.8}$$

and the mean potential density gradient is represented by

$$N_3 = g\left\{\frac{1}{\overline{\theta}_L}\frac{\partial \overline{\theta}_L}{\partial x_3} + \left[\frac{R_v}{R_a} - 1 + \left(\frac{L}{C_{pa}\overline{T}} - \frac{R_v}{R_a}\right)H(\overline{q}_c)\right]\frac{\partial \overline{q}_t}{\partial x_3}\right\}; \tag{2.9}$$

R_a and R_v are the gas constants for dry air and water vapour, C_{pa} is the specific heat at constant pressure for dry air, L is the latent heat of vaporization for water, and g is the gravitational acceleration. The mean total air (dry air plus water) density is given by

$$\bar{\rho} = \bar{p}/R_a\overline{T_v} \tag{2.10}$$

where the mean virtual temperature is

$$\overline{T_v} = \bar{T}\{1 + (R_v/R_a - 1)\overline{q_t} - (R_v/R_a)\overline{q_c}\}. \tag{2.11}$$

The mean temperature and mean cloud water specific humidity satisfy the algebraic equations

$$\bar{T} = \overline{\theta_L}(\bar{p}/p_0)^{R_a/C_{pa}} + L\overline{q_c}/C_{pa}, \tag{2.12}$$

$$\overline{q_c} = \max(0, \overline{q_t} - \gamma\overline{q_s}), \tag{2.13}$$

where the mean saturation specific humidity and the probability of cloud are

$$\overline{q_s} = (R_a/R_v)(p_{s0}/\bar{p}) \exp\{\alpha_{s0}(1 - T_{s0}/\bar{T})\}. \tag{2.14}$$

$$\gamma = \bar{q}_t^2/(\bar{q}_t^2 + |\overline{q_t'^2}|). \tag{2.15}$$

Clearly γ corresponds to the fractional cloud cover at a given height where there is some condensation.

The constants a_1, a_2, a_3, a_4, a_5, a_6, Ri_{crit}, p_0, p_{s0}, α_{s0} and T_{s0} are computed in Part I. Thus eqs. (2.1)–(2.15) form a closed system, whose solution by a finite element method is discussed below.

3. Method of solution

An approximate solution of a parabolic equation can be obtained by a finite element method (Manton, 1978b) which uses elements spanning both space and time. (This may be contrasted with the common finite element approach to time-dependent problems where only the spatial dependence is approximated by finite element methods; essentially finite difference methods are used for the time dependence (Zienkiewicz, 1971).) Let us consider a dependent variable v which satisfies the equation

$$\mathscr{L}(v, x_3, t) = 0. \tag{3.1}$$

Assuming that v at time $t = t_1$ is known at the set of mesh points $P(t_1) = \{x_3 = z_n(t_1)\colon n = 1, 2, \ldots, n_0\}$, we extrapolate the solution to $P(t_1 + \Delta t)$ by dividing the region $t \in [t_1, t_1 + \Delta t]$, $z \in [z_1, z_{n_0}]$ into trapezoidal elements with nodes $\{(z_n, t_1), (z_n, t_1 + \Delta t), (z_{n+1}, t_1), (z_{n+1}, t_1 + \Delta t)\colon n = 1, 2, \ldots, n_0 - 1\}$. Within each element, the variable v is approximated by

$$v^*(x_3,t) = \sum_{i=1}^{4} L_i(x_3,t)v_i, \tag{3.2}$$

where $\{v_i : i = 1, 2, 3, 4\}$ are the values of v^* at the nodes and $\{L_i : i = 1, \ldots, 4\}$ are given interpolation (or shape) functions. The shape function L_i is an hyperbola which increases linearly to unity along the sides including the ith node and which is zero along the other two sides. Thus (3.2) yields a linear interpolation in x_3 (or t) when t (or x_3) is fixed. Substitution of (3.2) into the left-hand side of (3.1) yields the residual $\mathscr{L}(v^*, x_3, t)$ which is not zero in general. An algebraic equation for v^* at each point in $P(t_1 + \Delta t)$ is obtained by setting

$$\int\int_\Omega W(x_3,t)\,\mathscr{L}(v^*,x_3,t)\,dx_3\,dt = 0, \tag{3.3}$$

where the region Ω consists of the two elements containing the given point and the weighting function W at a fixed t increases linearly from zero at the boundaries of Ω to unity at the common side of the two elements in Ω. Thus the extrapolation from $P(t_1)$ to $P(t_1 + \Delta t)$ involves the solution of a set of algebraic equations for the values of the dependent variable at the mesh points.

The interpolation (3.2) is linear in x_3 while the operator $\mathscr{L}$ contains terms involving the second derivative with respect to x_3. These terms in (3.3) are handled by use of the integral relation

$$\int_{t_1}^{t_2}\int_{z_1(t)}^{z_2(t)} W\frac{\partial}{\partial x_3}\left(K\frac{\partial v}{\partial x_3}\right)dx_3\,dt$$

$$= \int_{t_1}^{t_2}\left[WK\frac{\partial v}{\partial x_3}\right]_{z_1(t)}^{z_2(t)}dt$$

$$- \int_{t_1}^{t_2}\int_{z_1}^{z_2}\frac{\partial W}{\partial x_3}K\frac{\partial v}{\partial x_3}\,dx_3\,dt. \tag{3.4}$$

The first term on the right-hand side of (3.4) is zero because W is chosen to be zero on the boundaries $z_1(t)$ and $z_2(t)$. Thus the weighted residuals (3.3) can be expressed in terms of only first-order derivatives of the dependent variable over the interior of the elements.

An alternative method of ensuring that (3.3) contains only first-order derivatives is to introduce an additional dependent variable corresponding to $\partial v/\partial x_3$. Some tests with this latter method on the one-dimensional diffusion equation show that it produces much more accurate solutions than the former method. On the other hand, it doubles the number of dependent variables, thus increasing the amount of computation and storage of data. Therefore the former method is used in the present work.

The finite element method is used to solve the six eqs. (2.1)–(2.6). Although (2.6) is not a parabolic equation, a linear analysis shows readily that an accurate and stable solution is obtained from the present method (Manton, 1978b). Thus the pressure is determined in the same manner as the other dependent variables. (The method is absolutely stable also when applied to the linear advection equation $\partial v/\partial t + \partial v/\partial x_3 = 0$. Therefore the advection terms in the full system of equations described in Part I ought to be treated satisfactorily by the method. We note that conventional finite element methods can be used to solve the non-linear shallow-water equations (Cullen, 1974) and the steady-state Navier–Stokes equations (Laskaris, 1975).) Because the differential equations are non-linear, the set of algebraic equations for the dependent variables at $P(t_1 + \Delta t)$ (corresponding to (3.3)) is non-linear. The set is solved by iteration such that the coefficients in (2.1)–(2.6) are evaluated at the nth iteration using data from the $(n - 1)$th iteration. For the first iteration, the dependent variables at $P(t_1 + \Delta t)$ are set equal to those (known) values at $P(t_1)$ after having been smoothed to remove high wavenumber fluctuations. The smoothing is achieved with a three-point (1–2–1) filter applied to all internal nodes, and it reduces the accumulation of truncation error associated with boundary conditions especially. (Note that only the initial estimates of the variables at $P(t_1 + \Delta t)$ are filtered.) At each iteration there are $6n_0$ linear equations, where n_0 is the number of mesh points, and these are solved by Gaussian elimination. The coefficient matrix for these equations is banded because the weighted residuals (3.3) for a given mesh point involve only the adjacent mesh points. A considerable saving in computation and storage is obtained by storing only the non-zero band of the coefficient matrix; thus the effective coefficient matrix has dimensions $(6n_0 \times 24)$. Therefore the number of operations needed to solve the equations is proportional to n_0 rather than n_0^2.

Because the dependent variables are defined everywhere (not just at mesh points), the weighted residuals take into account the continuous variation of the variables. In particular, the occurrence of condensation over only some part of an element can lead to significant variations in $\overline{q_c}$ and $\bar{T}$ over that element. For this reason, it is advantageous not to have $\overline{q_c}$ and $\bar{T}$ as explicit dependent variables, which are restricted to linear interpolation. Although the interpolation functions for the dependent variables are algebraically simple, the evaluation of the integrals for the weighted residuals is not straightforward, especially when condensation occurs. We therefore use Gaussian quadrature to compute all the weighted residuals.

It is seen that all the coefficients in (2.1)–(2.6) can be calculated explicitly from (2.7)–(2.11) once the temperature $\bar{T}$ and cloud water $\overline{q_c}$ are determined from the coupled eqs. (2.12)–(2.15). Direct iteration on eqs. (2.12)–(2.13) does not necessarily converge: $\overline{q_c}$ can alternate between zero and some positive value. However, these equations can be solved easily. Setting

$$T_1 = \bar{\theta}_L(\bar{p}/p_0)^{R_a/C_{pa}}, \quad T_2 = L\overline{q_t}/C_{pa} \tag{3.5}$$

and

$$T_3 = \gamma(L/C_{pa})(R_a/R_v)(p_{s0}/\bar{p}),$$

we take $\bar{T} = T_1$ as a first approximation. If eqs. (2.13)–(2.15) now imply that $\overline{q_c} = 0$ then $\bar{T} = T_1$ and $\overline{q_c} = 0$ represent the solution of (2.12)–(2.15). If this is not the case then condensation occurs and the temperature is greater than T_1. From (2.12)–(2.15) and (3.5), the temperature is given by the implicit equation

$$\bar{T} - T_1 - T_2 + T_3 \exp\{a_{s0}(1 - T_{s0}/\bar{T})\} = 0. \tag{3.6}$$

Because the left-hand side of (3.6) is a monotonic increasing function of $\bar{T}$, the equation is solved rapidly by Newton-Raphson iteration. In practice, iteration is continued until the increment in $\bar{T}$ is less than δT, where δT equals 0.001 K. It is found that there is no discernible change in the dependent variables as δT is varied from 0.01 to 0.0001 K.

It is seen that eqs. (2.7) and (2.15) involve the moduli of E and $\overline{q_t'^2}$, although these functions are strictly positive. This is done because no constraint is put on the sign of the values of the dependent variables obtained from the solution method. Finite element methods tend to conserve the integral of a dependent variable and this is achieved by the mesh point values of the approximated variable being alternately greater and smaller than the exact solution. It is therefore natural for the finite element approximation of a variable to become negative when the exact form is near zero. No instability is associated with this process, and a variable always becomes positive as its magnitude increases from zero. An important consequence of not placing additional constraints on the dependent variables is that the solution method is applied to precisely eqs. (2.1)–(2.6); a constraint on the sign of E, say, means that the approximate solution for E at each point satisfies either (2.4) or the equation $E = 0$. Negative approximate values of scalar dependent variables are usually eliminated in finite difference methods (Deardorff, 1973), because they lead to numerical instabilities.

Being a parabolic system, eqs. (2.1)–(2.6) require all the dependent variables to be specified initially ($t = 0$) in order to extrapolate to later times. Although the initial values of $\overline{u_1}$, $\overline{q_t}$, E and $\overline{q_t'^2}$ may be chosen rather arbitrarily, we expect there to be constraints on the thermodynamic variables $\overline{\theta_L}$ and $\bar{p}$: $\overline{\theta_L}$ controls the static stability of the fluid layer while $\bar{p}$ ought to be approximated by the stress due to the weight of the layer. The initial values of $\overline{\theta_L}$ and $\bar{p}$ therefore are computed from a given nominal mean temperature (T_{nom}) by assuming that the atmosphere is dry and in static equilibrium. The nominal temperature field is piecewise linear and so we have for the layer $x_3 \in (z_m, z_{m+1})$

$$\bar{p} = p_m\{1 - (x_3 - z_m)/d_m\}^{(gd_m/R_a T_m)},$$

$$\overline{\theta_L} = T_{\text{nom}}(p_0/\bar{p})^{R_a/C_{pa}}, \tag{3.7}$$

where $T_{\text{nom}} = T_m\{1 - (x_3 - z_m)/d_m\}$.

The pressure and temperature are assumed to be continuous functions of x_3. Thus only the layer base (z_m) and the lapse rate ($-T_m/d_m$) need to be specified for each layer, except that T_m and p_m are given at the ground ($x_3 = 0$). It is clear that the nominal temperature corresponds to the actual temperature only when there is no water in the air.

A unique solution of (2.1)–(2.6) requires two boundary conditions for each of the variables $\overline{u_1}$, $\overline{\theta_L}$, $\overline{q_t}$, E and $\overline{q_t'^2}$; one boundary condition is needed on $\bar{p}$. Boundary conditions are applied in general at the mid-points of boundary elements. This is achieved readily because the variables change linearly across an element, and it allows Dirichlet and Neumann boundary conditions to be applied consistently. Flux boundary conditions can be applied very accurately by using the formally computed value of the eddy diffusivity at the mid-point of an element.

Although the finite element method can be used with a completely arbitrary mesh, a fixed time increment and a fixed (but non-uniform) spatial mesh is used in all the results discussed below. This constraint implies that the elements are rectangles rather than trapezia. While there may be some advantage in allowing the spatial mesh to vary with time (in order to follow an inversion, for example), the computation time of a problem is increased by determining the location of the mesh points at each time and by integrating over trapezia rather than rectangular elements.

4. Test problem

In order to check the internal consistency of the solution method described in Section 3, we consider an artificial problem which involves the development of condensation, shear and turbulent diffusion within a relatively short time. Tests can therefore be carried out succinctly. The nominal temperature field (3.7) is neutrally stable (with a lapse rate of 9.75 K km^{-1}) up to 300 m, where there is a strong inversion (T_{nom} increases by 1 K over 50 m); the air above 350 m is stable with a lapse rate of 5 K km^{-1}. The total water specific humidity initially has a constant value of 8 g kg^{-1} up to a height of 350 m; it then decreases linearly to zero so that there is no water above 400 m. It follows from the nominal temperature field that there is cloud water between 140 and 360 m, with a maximum value of 0.28 g kg^{-1} at 300 m. The initial profile of the mean velocity increases logarithmically (strictly, only the values of $\overline{u_1}$ at mesh points increase logarithmically) up to 350 m and it is constant above 350 m. At mesh points for $x_3 < 350$ m, we have

$$\overline{u_1} = (u_*/k)\ln(x_3/z_0),$$

where $u_* = 40$ cm s^{-1} and $z_0 = 1$ cm; hence $\overline{u_1}$ equals 11.96 m s^{-1} above 350 m. The turbulent energy E initially decreases linearly from u_*^2/a_1

(which corresponds to a neutral equilibrium surface layer) at the first mesh point and it is zero above 350 m. The variance $\overline{q_t'^2}$ is set equal to zero at $t = 0$.

The spatial domain extends from 5 to 2000 m and the first element has nodes at x_3 equals 5 and 10 m. Hence the lower boundary conditions are applied at 7.5 m. Here $\overline{u_1}$, $\overline{q_t}$ and E are kept constant at their initial values, $\overline{\theta_L}$ decreases at a constant rate of 3.6 K/h, while the gradient of $\overline{q_t'^2}$ is equal to zero. Thus the lower boundary conditions correspond to the mixed layer being cooled and stabilized. The upper boundary is assumed to remain undisturbed; all the variables are kept constant at their initial values.

There is no horizontal pressure gradient (i.e. $\partial\bar{p}/\partial x_1 \equiv 0$ in (2.1)). Consistent with the neglect of Coriolis forces, the mean flow is driven by the specification of $\overline{u_1}$ at the upper and lower boundaries. If the Coriolis forces were present then the geostrophic wind in the upper layers and the frictional forces at the ground would balance the horizontal pressure gradient.

The equations are integrated from $t = 0$ to $t = 3000$ s, and various comparisons are made at the final time. The dependence of the solution upon the time and space mesh sizes is investigated in Section 5. The solution method involves two sources of truncation error: the integration of the weighted residuals is done numerically and the non-linear algebraic equations for the dependent variables at mesh points are solved iteratively. These effects also are considered below.

5. Results

The problem posed in Section 4 is solved using a CDC CYBER 7600 computer. The run time varies approximately linearly with the number of mesh points, the number of time steps and the number of iterations used to solve the non-linear algebraic equations at each time. It increases with the square of the number of dependent variables (fixed at six) and the square of the order of the Gaussian quadrature. A computation using 31 mesh points, a time step of 300 s, four iterations of the equations and four-point integration takes nearly 7 s.

The problem involves initially a moist mixed

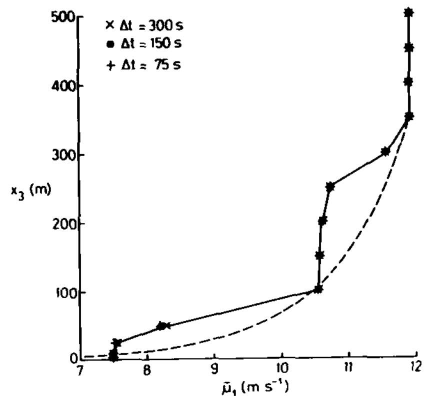

Fig. 1. Dependence of mean wind profile $\overline{u_1}(x_3)$ at $t = 3000$ s upon time step. ----- $\overline{u_1}$ at $t = 0$.

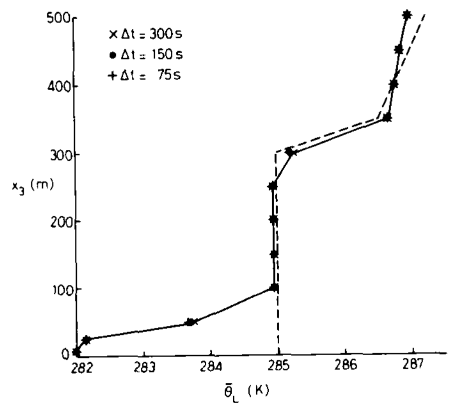

Fig. 2. Dependence of potential temperature profile $\overline{\theta_L}(x_3)$ at $t = 3000$ s upon time step. ----- $\overline{\theta_L}$ at $t = 0$.

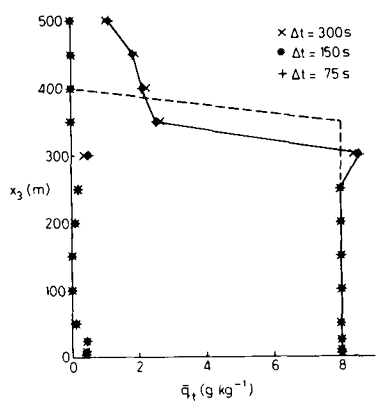

Fig. 3. Dependence of total water profile $\overline{q_t}(x_3)$ at $t = 3000$ s upon time step; isolated points represent cloud water specific humidity $\overline{q_c}$. ----- $\overline{q_t}$ at $t = 0$.

layer which is capped by an inversion at 300 m and which has cloud from about 150 to 350 m. The initial distributions of $\overline{u_1}$, $\overline{\theta_L}$ and $\overline{q_t}$ are shown in Figs. 1, 2 and 3. Two (somewhat unrealistic) anomalies are seen: the high value of the water content extends 50 m above the inversion and the mean velocity varies smoothly over the whole layer. As time increases, the water directly above the inversion diffuses upward and a mean shear develops at the inversion. The air at the lower boundary is steadily cooled and so the surface layer (up to about 25 m) is stabilized. This tends to suppress the turbulence in the surface layer, uncoupling it from the higher level motion. Because the mean velocity is fixed at the lower boundary, the suppression of the turbulence is associated with a lack of mean shear in the surface layer. Just above this layer there is a very strong shear as the velocity increases from about 7 m s^{-1} to 10.5 m s^{-1}. Turbulence is suppressed also in this region because $\overline{\theta_L}$ increases very rapidly. The cooling of the surface layer and the maintenance of the total water content lead to the condensation of water near the ground. This evolution of the boundary layer occurs gradually over about 2400 s, and Figs. 1, 2 and 3 show the situation at $t = 3000$ s. Subsequent integration of the equations to $t = 7200$ s shows that there is little further development, except that there is a steady increase in the amount of liquid water in the surface layer. It is seen that at least the qualitative behaviour of the model is physically sound. However, our emphasis here is on the accuracy of the solution method.

The validity of the specification (2.15) for the fractional cloud cover is not studied. In fact γ is greater than 0.99 throughout the calculation because $\overline{q_t'^2}$ is small. It is seen from (2.5) that total water variance is generated particularly in regions of large total water gradient and high turbulence level. Near the ground there is no total water gradient and so $\overline{q_t'^2}$ is invariably less than 0.01 g^2 kg^{-2}. Although there is a strong gradient in $\overline{q_t}$ at the inversion, the turbulence level is low because it is not sustained by convection from the ground. Moreover, the maximum value of $\overline{q_t'^2}$ (less than 1 g^2 kg^{-2}) occurs above the inversion where $\overline{q_t}$ itself is small compared with the saturation specific humidity.

All tests with the method yield an oscillation in $\bar{p}$ at the lowest levels with a frequency of twice the time step and a magnitude of about 0.5 mb. This is not an instability: the magnitude of the oscillation does not increase with time. As discussed in Section 3, finite element methods tend to cause the mesh-point values of a dependent variable to be alternately greater and smaller than the exact value; thus the integral of the value is conserved. The pressure is obtained by integrating (2.6) down from 2000 m where its value is specified, and so its value at the lowest mesh point is relatively unconstrained.

To test the sensitivity of the solution to the order of the Gaussian integration and the number of iterations used in solving the algebraic equations, we set the time step at 300 s and take 31 mesh points located as follows: 5 m, 10 m, 25 m, 50 m, thence to 1000 m at 50-m intervals; eight points are distributed logarithmically between 1000 and 2000 m. Thus the mesh size is 50 m over the body of the flow. Taking four iterations of the algebraic equations, we first consider the solution at $t = 3000$ s as the order of the integration is varied from two to eight. It is found that the solution at each mesh point does not necessarily converge monotonically with an increasing number of integration points, and that convergence is slowest in regions of most rapid change (i.e. between 25 and 100 m and between 300 and 400 m). Setting eight-point integration as a standard, we observe that the "errors" in four-point integration are generally small: $\overline{u_1}$ varies by no more than 1 cm s^{-1}, $\overline{\theta_L}$ by 0.02 K, $\overline{q_c}$ by 0.03 g kg^{-1} and $\overline{q_t}$ by 0.05 g kg^{-1}, except at 350 m, where there is a difference of 0.1 g kg^{-1}. The total water at 350 m drops from 8 g kg^{-1} at $t = 0$ to about 2.6 g kg^{-1} at $t = 3000$ s, and $\overline{q_t}$ at 3000 s decreases from about 8.5 g kg^{-1} at 300 m to 2.6 g kg^{-1} at 350 m. Thus the large error in q_t occurs at the point where it changes most significantly in space and time. Because two-point and three-point integrations yield somewhat larger errors (e.g. the maximum error in $\overline{\theta_L}$ increases to 0.09 K), we use four-point integration in all the following calculations.

The dependence of the solution upon the number of iterations of the algebraic equations is now discussed. Once again the convergence of the solution at each mesh point is not necessarily monotonic. The slowest convergence occurs on the elements between 50 and 100 m and between 300 and 350 m where the variables change most rapidly. This suggests that these elements are really too large to accommodate properly the required variations.

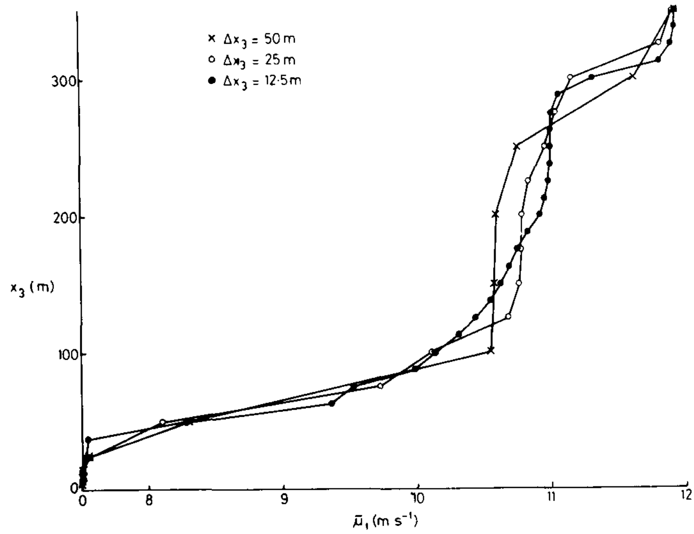

Fig. 4. Dependence of mean wind profile $\overline{u_1}(x_3)$ at $t = 3000$ s upon mesh size; $\Delta t = 300$ s.

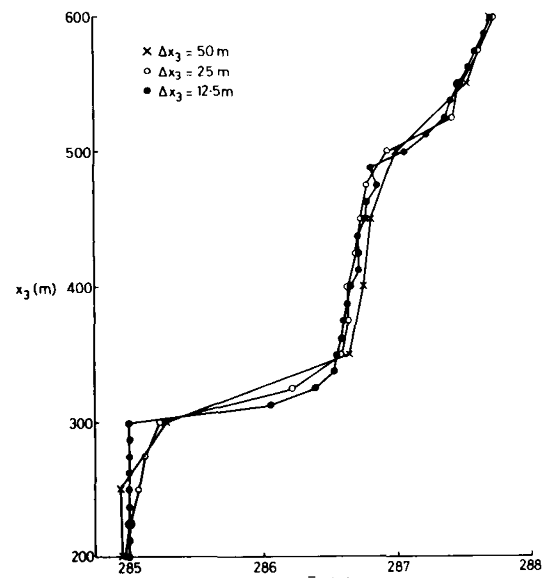

Fig. 5. Dependence of potential temperature profile $\overline{\theta_L}(x_3)$ at $t = 3000$ s upon mesh size; $\Delta t = 300$ s.

However, if the 15-iteration solution is taken as a standard then the maximum "errors" in the four-iteration solution at $t = 3000$ s are 5 cm s^{-1} in $\overline{u}_1$, 0.06 K in $\overline{\theta_L}$, 0.15 g kg$_{-1}$ in $\overline{q_t}$, 0.05 g kg^{-1} in $\overline{q_c}$ and 0.15 K in $\overline{T}$. In all the following calculations the algebraic equations are iterated four times.

The chosen calculation criteria (four-point Gaussian quadrature and a four-iteration solution of the algebraic equations) are considered to be conservative. Less stringent criteria can yield solutions with maximum errors which are no greater than those in the solutions using the chosen criteria. It is remarkable that even a one-iteration solution (which perhaps could be compared with a forward time difference solution) is completely stable, and it yields maximum errors not significantly greater than those in higher-order solutions. On the other hand, the chosen criteria lead to solutions with little or no discernible error on elements over which the variables do not change extremely rapidly.

The sensitivity of the solution to the magnitude of the time step is studied by solving the problem (with 31 mesh points) with a time step (Δt) of 300, 150 and 75 s; the results are shown in Figs. 1, 2 and 3. The solution clearly does not depend strongly upon the time step. Taking $\Delta t = 75$ s as a standard, we see that the maximum errors when $\Delta t = 300$ s are 9 cm s^{-1} in $\overline{u_1}$ at 50 m, 0.07 K in $\overline{\theta_L}$ at 300 m, 0.20 g kg^{-1} in $\overline{q_t}$ at 300 m and 0.10 g kg^{-1} in q_c at 300 m. These errors occur on elements where the variables change most rapidly. The maximum errors when $\Delta t = 150$ s are 4 cm s^{-1} in $\overline{u_1}$, 0.03 K in $\overline{\theta_L}$, 0.02 g kg^{-1} in $\overline{q_t}$ and 0.01 g kg^{-1} in $\overline{q_c}$. The solution therefore appears to converge rapidly with decreasing time step.

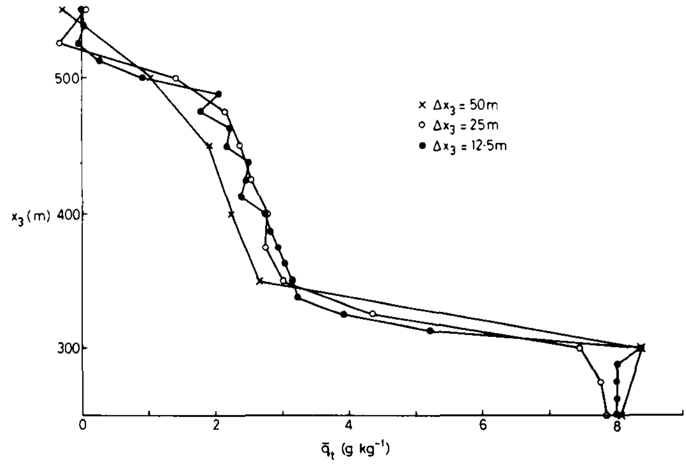

Fig. 6. Dependence of total water profile $\bar{q}_t(x_3)$ at $t = 3000$ s upon mesh size; $\Delta t = 300$ s.

The dependence of the solution upon the mesh size is investigated by solving the problem (with $\Delta t = 300$ s) with 31, 51 and 101 mesh points respectively. The first case has mesh points at 5, 10, 25 and 50 m and then has a mesh size (Δx_3) of 50 m over the region 50 to 1000 m (as described above), while the second has a mesh size of 25 m from 25 m to 1000 m. The last case has an additional mesh point at 15 m and a mesh size of 12.5 m over the region from 25 to 1000 m with a further 19 mesh points logarithmically distributed between 1000 and 2000 m. It is found that there is good agreement between the solutions; profiles of $\bar{u}_1$, $\bar{\theta}_2$ and $\bar{q}_t$ are shown in Figs. 4, 5 and 6. (Note that the small negative values of $\bar{q}_t$ above 500 m in Fig. 6 are not unexpected, as discussed in Section 3. As the magnitude of $\bar{q}_t$ at a given height increases with time, $\bar{q}_t$ becomes positive definite and it varies smoothly.) It is seen that the coarse resolution solution ($\Delta x_3 = 50$ m) is essentially a running average of the finer resolution solutions, which involve a considerable amount of structure with scales less than 50 m. The maximum differences between the 50 and 12.5 m solutions are 41 cm s^{-1} in $\bar{u}_1$, 0.27 K in $\bar{\theta}_L$, 0.5 g kg^{-1} in $\bar{q}_t$ and 0.07 g kg^{-1} in $\bar{q}_c$. For the 25 and 12.5 m solutions, these differences drop to 27 cm s^{-1} in $\bar{u}_1$, 0.23 K in $\bar{\theta}_L$, 0.19 g kg^{-1} in $\bar{q}_t$ and 0.06 g kg^{-1} in $\bar{q}_c$, except at 300 m where $\bar{q}_t$ for the 25 m solution is 0.93 g kg^{-1} lower than that for the 12.5 m solution and this causes $\bar{q}_c$ to be 0.45 g kg^{-1} lower. Away from the point $x_3 = 300$ m, the 25 m solution follows closely the detailed structure of the 12.5 m solution.

6. Well-mixed layers

The model equations derived in Part I involve an eddy viscosity and this may raise some doubts as to the ability of the model to represent well-mixed layers which are produced in stably stratified fluids by turbulence applied at a horizontal boundary. A common method of generating well-mixed layers in the laboratory (Turner, 1973) is to oscillate a horizontal grid of metal bars in order to produce turbulence which propagates through the layer to an inversion. One of the first experiments of this type is that of Cromwell (1960) in which a grid is oscillated in a tank of water with an initially linear density gradient. We now demonstrate that such a mixed layer can be represented by the model equations.

We consider a layer of air in which there is no mean horizontal motion ($\bar{u}_1 \equiv 0$) and no water ($\bar{q}_t \equiv 0$). At time $t = 0$, a well-mixed layer with a lapse rate of 9.75 K/km extends to a height of 350 m and it is capped by a stable layer with a lapse rate of 5 K/km. The turbulent energy E initially decreases linearly from 5000 cm^2 s^{-2} at 7.5 m to zero at 350 m. The boundary values of all the variables are kept constant for all times. The problem is solved using the spatial grid with $\Delta x_3 = 25$ m and a time step of 300 s, as described in Section 5 above.

The profiles of $\bar{\theta}_L$ and E at time $t = 3000$ s are shown in Figs. 7 and 8. The mixed layer is seen to have increased its initial depth by about 50 m and it is capped by a sharp inversion. The turbulent energy decreases monotonically with height and

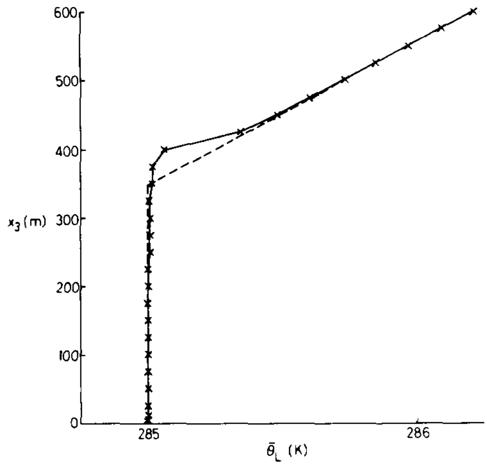

Fig. 7. Potential temperature profile $\bar{\theta}_L(x_3)$ in well-mixed layer at time $t = 3000$ s. ------ $\bar{\theta}_L$ at $t = 0$.

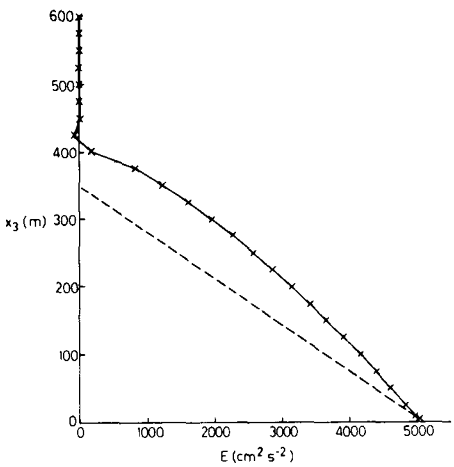

Fig. 8. Turbulent energy profile $E(x_3)$ in well-mixed layer at time $t = 3000$ s. ----- E at $t = 0$.

falls to essentially zero at the top of the mixed layer. (The small negative values of E above 400 m are present because E is not constrained to be positive, as discussed in Section 3. They do not lead to any numerical instability and they are eliminated as the magnitude of E increases.) The ability of the model equations, despite the use of an eddy diffusivity, to represent well-mixed layers is that the diffusivity depends explicitly upon the turbulent energy which is itself predicted explicitly. Thus turbulent energy can be transported readily from one region of the flow to another. In the present example, E diffuses from the lower boundary to the inversion where it entrains fluid from the stable layer above. Turbulence above the inversion is suppressed by the strong stable density gradient. Similar results are found for a well-mixed layer generated by a positive heat or total water flux at the lower boundary.

7. Conclusions

Equations governing the behaviour of the first moments of the dependent variables in moist, deep convection are derived in Part I of this work. In the present paper, a finite element method, using elements which span both time and space, is used to solve these equations for a one-dimensional boundary layer. An artificial problem is chosen in order to test succinctly the consistency of the solution method. The flow consists initially of a moist mixed layer capped by an inversion. There is an anomalously high amount of water directly above the inversion and the mean wind increases smoothly over the whole layer. The flow develops by diffusing the water anomaly upward and by forming a mean shear across the inversion. Cooling at the ground leads to stabilizing of the surface layer and to condensation near the surface. These features of the solution are reproduced well and the solution does not depend significantly upon the time step (taken to be 300 s or less) or the mesh size (taken to be 50 m or less over the body of the domain). It is also demonstrated that the model equations, despite the use of an eddy viscosity, can represent the deepening of well-mixed layers.

REFERENCES

Cromwell, T. 1960. Pycnoclines created by mixing in an aquarium tank. *J. Mar. Res. 18*, 73.

Cullen, M. J. P. 1974. Integrations of the primitive equations on a sphere using the finite element method. *Q. J. R. Meteorol. Soc. 100*, 555.

Deardorff, J. W. 1973. The use of subgrid transport equations in a three-dimensional model of atmospheric turbulence. *J. Eng. Fluids 95*, 429.

Kolmogorov, A. N. 1942. Equations of turbulent motion of an incompressible turbulent fluid. *Izv. Akad. Nauk SSSR Ser. Phys. VI*, No. 1–2, 56.

Laskaris, T. E. 1974. Finite element analysis of compressible and incompressible viscous flow and heat transfer problems. *Phys. Fluids 18*, 1639.

Manton, M. J. 1978a. A finite element model of a moist atmospheric boundary layer: Part I—model equations. *Tellus 30*, 219.

Manton, M. J. 1978b. On the solution of initial value problems by finite element methods. Submitted for publication.

Turner, J. S. 1973. *Buoyancy effects in fluids*, Cambridge Univ. Press.

Walsh, J. E. 1974. Sea breeze theory and applications. *J. Atmos. Sci. 31*, 2012.

Wyngaard, J. C. and Coté, O. R. 1974. The evolution of a convective planetary boundary layer—a higher-order-closure model study. *Boundary-Layer Meteorol. 7*, 289.

Yamada, T. and Mellor, G. L. 1975. A simulation of the Wangara atmospheric boundary layer data. *J. Atmos. Sci. 32*, 2309.

Zienkiewicz, O. C. 1971. *The finite element method in engineering science*. McGraw-Hill.

КОНЕЧНО-ЭЛЕМЕНТНАЯ МОДЕЛЬ ВЛАЖНОГО ПОГРАНИЧНОГО СЛОЯ АТМОСФЕРЫ: ЧАСТЬ II — МЕТОД РЕШЕНИЯ

Представлена конечно-элементная модель для решения системы уравнений, описывающей поведение глубокой влажной конвекции. Метод использует элементы, охватывающие как время, так и пространство, причем могут быть использованы переменные шаги по времени и пространству. Уравнение для давления решается точно также, как и уравнения для других зависимых переменных. Решается задача об искусственном одномерном течении в пограничном слое, в котором перемешанный слой, ограниченный сверху инверсией, стабилизирован охлаждением подстилающей поверхности. Найдено, что решение не зависит существенно от шага по времени или по пространству.